APPLIED RESEARCH

Flexible Thin Film-Based Triple Port UWB MIMO Antenna With Modified Ground Plane for UWB, WLAN, WiMAX, WPAN and 5G Applications

PAITOON RAKLUEA [1], **NORAKAMON WONGSIN** [1], (Member, IEEE),
CHATREE MAHATTHANAJATUPHAT [2], (Member, IEEE), **PONGSATHORN AROONMITR** [1],
THINNAWAT JANGJING [1], **CHAWALIT RAKLUEA** [1], (Member, IEEE),
WANCHALERM CHANWATTANAPONG [1], **AND NONCHANUTT CHUDPOOTI** [3], (Member, IEEE)

[1]Department of Electronics and Telecommunication Engineering, Faculty of Engineering, Rajamangala University of Technology Thanyaburi (RMUTT), Khlong Hok, Pathum Thani 12110, Thailand
[2]Department of Electrical and Computer Engineering, Faculty of Engineering, King Mongkut's University of Technology North Bangkok, Bangkok 10800, Thailand
[3]Department of Industrial Physics and Medical Instrumentation, Faculty of Applied Science, King Mongkut's University of Technology North Bangkok, Bangkok 10800, Thailand

Corresponding authors: Norakamon Wongsin (norakamon@rmutt.ac.th) and Chatree Mahatthanajatuphat (chatree.m@eng.kmutnb.ac.th)

ABSTRACT This manuscript presents a triple-port ultra-wideband (UWB) multiple-input multiple-output (MIMO) antenna designed for wireless communication. The antenna employs automobile window film as a substrate, which is a cost-effective, easily accessible, and ultra-thin material. The proposed structure comprises a monopole antenna featuring a circular patch pattern that is fed by a coplanar waveguide (CPW). Additionally, the internal ground plane has been modified by grooving both sides to form a rectangular slot antenna construction. As a result, the antenna possesses identical dimensions and is equipped with three ports. The antenna exhibits a frequency range spanning from 3.1-GHz to 10.6-GHz across all three ports. Additionally, the $|S_{11}|$ at port 1 demonstrates an extensive operating bandwidth of 2.4-GHz to 10.6-GHz with a signal attenuation of less than -10-dB. Consequently, it has the capability to facilitate a diverse range of applications such as ultra-wideband (UWB), Worldwide Interoperability for Microwave Access (WiMAX), Wireless Personal Area Network (WPAN), Wireless Local Area Network (WLAN), and 5G. Furthermore, the antenna exhibits a gain of 5.8 dBi across its entire range, a correlation coefficient below 0.45, and a group latency of under 0.85 ns. The antenna exhibits both omnidirectional and bidirectional radiation patterns across its operational range at ports 1, 2, and 3.

INDEX TERMS IMIMO, ultra-wideband, thin film, triple port, modify ground, rectangular slot.

I. INTRODUCTION

Currently, wireless communication technology has advanced to a stage where various devices can communicate and collaborate through different types of connections. These connections include Wireless Local Area Network (WLAN), which is a local area connection facilitated by access points,

The associate editor coordinating the review of this manuscript and approving it for publication was Ravi Kumar Gangwar [ID].

as illustrated in [1]. Additionally, Wireless Personal Area Network (WPAN) connections link devices within an individual's vicinity, as depicted in [2] and [3]. Furthermore, Wireless Body Area Network (WBAN) connections enable communication between network equipment on the human body and measuring instruments, as demonstrated in [4] and [5]. The Federal Communications Commission (FCC) has approved Ultra-wideband (UWB) as a low-power, high-bandwidth transmission method with an operating frequency

range of 3.1 GHz to 10.6 GHz. Despite its short transmission distance of 10.6 GHz [6], UWB utilizes Multiple-Input and Multiple-Output (MIMO) technology to increase the capacity of the channel. This technology can support a variety of applications and improve the efficiency of applications that require high-speed data transfer.

Previous studies have presented the notion of antenna analysis and production for Ultra-Wideband (UWB) technology. This includes the development of antennas on diverse materials to facilitate a range of wireless communications. According to the proposal by [7], a 3-port antenna can be constructed using FR-4 as the base material. The study's findings indicate that the three ports function effectively in LTE band 42, exhibiting satisfactory isolation, and do not necessitate a modular configuration. The article referenced in [8] showcases antennas that utilize Roger RT/Rudoid 5880 as a base material. These antennas cover a range of operating frequency bands, from microwave (2.5, 3.5, 5.5, and 7.5 GHz) to millimeter wave (23 - 31 GHz), and boast a radiation efficiency of over 95% and a stable gain of > 2.5 dBi at the microwave band and 6.5 dBi at the millimeter band. These features make them well-suited for 5G IoT applications, particularly in the areas of smart homes, offices, and vehicle-to-everything communications. The article referenced as [9] describes a functional module for a 4-port MIMO antenna in capsule endoscopy. The module utilizes a Rogers RO4003 plate as the base material and is designed to enable real-time transmission of high-resolution images at high data rates. It is evident that the foundational material utilized in references [7], [8], and [9] is a rigid substance possessing high durability but lacking flexibility. As a result, there has been a development and application of materials that offer greater flexibility.

The study in [10] describes a wideband MIMO antenna using a polyester fabric basis. The product's high flexibility allows for successful installation on curved or bent surfaces, and it can be utilized for wear within a frequency range of 2 GHz to 30 GHz. This includes support for 5G frequencies such as 2.6 GHz and 26 GHz, as well as WBAN applications ranging from 2.4 GHz to 10.6 GHz. Additionally, it is deemed appropriate and exhibits optimal performance in wearables or blankets of the Wireless Body Area Network (WBAN) category. However, this particular specialization may not be adequately suited for outdoor or other applications as required. Film-type base materials present an intriguing alternative. The film exhibits excellent resistance to high temperatures and humidity, making it suitable for use in diverse weather conditions. The paper in [11] describes a multi-band antenna designed for WLAN and LTE MIMO systems. The antenna employs a thin-film base material with a dielectric constant of εr of 3.2 and a thickness of 0.3 mm. The device supports multiple frequency bands, including WLAN band at 2.4 GHz, LTE 1800 MHz Band 3 with UL 1710 MHz - 1785 MHz and DL 1805 MHz - 1880 MHz, LTE 2100 MHz Band 1 with UL 1920 MHz - 1980 MHz and DL 2110 MHz- 2170 MHz, as well as LTE 2300 MHz band

40 at 2300 MHz - 2400 MHz and LTE 2600 MHz band 38 at 2570 MHz - 2620 MHz. In [12], a carbon black film was utilized to enhance the separation of MIMO antenna systems in UWB systems. The findings suggest that the film has the potential to be utilized in diverse MIMO systems. The author proposes the utilization of carbon black film, specifically automotive window film, as the foundational material for the design and construction of the antenna.

Regarding the implementation of MIMO technology, a compact 4-port planar UWB array antenna is presented in [13]. The simulation outcomes and the measurements of the workpiece both suggest that the antenna exhibits satisfactory performance. The MIMO performance of the array antenna is demonstrated to be good based on the correlation coefficient and channel capacity loss. The present paper, referenced as [14], introduces a novel approach for designing a 2-port MIMO antenna system for UWB applications. The proposed method employs a specially engineered material to achieve miniaturization and optimal performance of both antennas, which are intended to operate in MIMO systems. The design technique utilizes the Split-Ring Resonator (SRR) technique on the patch plane. In reference to [15], the paper presents an appropriate choice for a variety of system requirements, including future UWB and WLAN systems. The design features a reconfigurable 3-port monopole antenna with 3 switchable states, making it suitable for UWB and WLAN applications at 2.4 GHz and 5.8 GHz frequencies. Additionally, the article referenced as [16] presents a compelling 3-port MIMO antenna designed for a novel, space-saving UWB system. The prototype antenna comprises a circular monopole antenna that is fed by a coplanar waveguide (CPW) with an identical ground plane structure. This design utilizes the ground plane as a microstrip antenna, eliminating the need for any separate elements. In a subsequent publication [17], a concise two-port MIMO antenna was introduced for UWB applications. The antenna was fabricated using a thin-film substrate material to minimize its thickness. This feature enables efficient performance on surfaces with curved geometries. In the design, a film thickness of approximately 0.056 mm was utilized in combination with square channel and rectangular stub antennas. The results indicated that the antenna is suitable for employment in a variety of communication systems, including WPAN, WLAN, and UWB.

Researchers have focused on the development of communications in the automobile industry, as referenced in [18], [19], [20], [21], [22], [23], and [24]. In accordance with the development of electric cars, communication technologies in the automotive sector are now receiving a lot of attention. There is growing anticipation for the emergence of autonomous vehicle technologies. However, this necessitates the optimization of high-precision, low-latency data traffic to fully realize its potential. Given that passenger safety is at stake, it is imperative to ensure that the antenna, which serves as the crucial component responsible for transmitting and receiving data between devices, is optimized to meet these

expectations. The aforementioned publication [18] details a multi-band monopole antenna designed for use in automotive applications within Long-Term Evolution (LTE) and 5G systems. The antenna is capable of covering a frequency range spanning from 617 MHz to 5 GHz while maintaining a reasonable level of rejection at L1/L2/L5 GNSS bands. The device is mounted within the Shark-Fin located on the roof of the vehicle. The paper in regard [19] presents multiple-input multiple-output (MIMO) antennas designed for use in automotive applications. The configuration comprises a monopole with two hemispherical load slots and a staircase grounding, situated on a glass substrate measuring 29 × 50 mm. Fluorine-doped Tin Oxide (FTO) and Indium-doped Tin Oxide (ITO) serve as conductive layers on the top and bottom of the substrate, respectively. The product is intended for attachment onto the glass surface of a vehicle. The article referenced as [20] introduced a prospective antenna designed for the automotive radar that utilizes Ridge Gap Waveguides (RGWs) technology. The aforementioned structure comprises eight U-shaped slots that function within the frequency range of 76-81 GHz. The purpose of the article referenced as [21] is to investigate the impact of road surface, vehicle environment, and vehicle on the transmission of the dual-band microwave antenna. The product underwent testing on automotive components to evaluate its performance in Cellular-Vehicle to Everything (C-V2X) communications at frequencies of 975 MHz and 5.5 GHz. The article in [22] presents a concise design of a multiple-input multiple-output (MIMO) antenna suitable for sub-6GHz 5G applications in vehicles. The antenna has been designed with a Partial Ground Plane (PGP) structure on an FR4 substrate, featuring two ports and a monopole configuration. This is an excellent choice for installation within a Shark-Fin. The paper indicating [23] introduces a MIMO quad-element antenna that operates in the UWB range. The antenna features a hexagonal monopole structure with microstrip cable feeding arranged perpendicularly. Resonances at 1.5 GHz and 2.45 GHz were achieved by incorporating E-shaped and G-shaped stubs. According to the authors, the technology can be employed in diverse automotive applications such as vehicle-to-vehicle (V2V), vehicle-to-infrastructure (V2I), vehicle-to-everything (V2X), intelligent transport systems (ITS), automatic vehicle identifier, and RFID-based electronic toll collection. A MIMO antenna for UWB 12 ports was proposed in reference [24]. This antenna is capable of covering the frequency ranges of GSM and Bluetooth. The antenna is designed using a 4-element horizontal and 8-element vertical arrangement, based on a simple rectangular monopole antenna. The dimensions of the antenna are 100×100 mm^2. One advantage is the availability of a range of polarization options. The product has undergone testing and has been found to be appropriate for utilization in automotive applications.

The dimensions and adaptability of automotive applications continue to be significant aspects to take into account. Consequently, our primary objective is to develop antennas suitable for use in the automobile sector. The optimal

FIGURE 1. The proposed antenna application on the automobile.

location for the installation of the antenna is the windshield region. Hence, to ensure the aesthetically pleasing and suitable integration of the antenna structure with the windscreen surface, proper design measures need to be included. Additionally, it has the characteristic of flexibility in accordance with curvature, so alleviating the load imposed on the windshield by the antenna. Hence, the suggested antenna utilizes a lightweight and flexible material, like that of a vehicle film, as its foundational component. This paper presents an alternative approach to designing a versatile 3-port MIMO antenna that is compatible with various wireless communication systems such as UWB, WLAN, WiMAX, WPAN, and 5G applications. The proposed antenna will utilize a car window film as an antenna substrate. That is an excellent basis material since it is incredibly thin, flexible, affordable, and readily accessible. The proposed antenna structure comprises a circular patch pattern monopole antenna that is fed by a co-planar waveguide with the ground and encloses a square patch cavity antenna. Based on the simulation and measurement results, it is indicated that the proposed antenna is suitable for use in automotive wireless communication applications. The evaluation of antenna performance simulations is conducted through the utilization of the CST program. This antenna provides dispersion patterns that are both omnidirectional and bidirectional. Furthermore, the antenna being discussed covers a frequency range of 2.4 GHz to 10.6 GHz, making it suitable for a range of vehicle applications including 5G, UWB, WPAN, WiMAX, and WLAN, as illustrated in Fig. 1. This proposed antenna was designed and evaluated for its reflection coefficient characteristics using actual car windows to assess its impact on the operating frequency.

The present research paper comprises the subsequent sections: The second section of the report delves into the antenna design and evaluates the simulation outcomes. This includes an examination of the impact of modifications to the antenna structure parameters, as well as an assessment of the antenna surface current distribution at various frequencies. Section III

FIGURE 2. Measuring the characteristics of a thin-film.

presents the measured antenna characteristics of the prototype antenna and the prototype antenna installed on the windshield. Lastly, section IV provides a comprehensive overview of the findings obtained from the research.

II. ANTENNA DESIGN AND ANALYSIS

A. ULTRA-WIDEBAND MIMO ANTENNA DESIGN

The motivation behind the antenna design was to create a flexible antenna that can easily conform to various surfaces, including automobile glass, to facilitate straightforward installation. As a result, the carbon black window film of the automobile was employed as the substrate for the antenna. As depicted in Fig. 2, the necessary design parameters, including the relative dielectric constant (ε_r) of 3.2, thickness (h) of 0.056 mm, and loss tangent (tanδ) of 0.016, were obtained through measurement. Furthermore, the automotive film is coated with a conductive substance comprising of copper tape, which has a thickness of 0.07 mm and a conductivity (σ) value of 5.8×10^7 S/m. The construction of the prototype monopole antenna is illustrated in Fig. 3. The proposed antenna is comprised of a conductive sheet material that is formed by combining a circular plate with a radius of R and a modified ground plane on both sides. The monopole radiator, having an electrical length of ($2 \times R$) approximately $\lambda_g/4$, is mounted on a thin-film substrate and powered by a coplanar waveguide (CPW) having an impedance of 50Ω, as specified by port 1.

Furthermore, the ground plane underwent modification through the creation of a slot by grooving on both sides, which led to the propagation of horizontal waves. The electrical length of each ground plane slot is approximately equal to λ_0. The altered ground patches were supplied with a 50-ohm impedance by CPW, in accordance with the requirements of ports 2 and 3. Especially, the transmission line of the antenna is configured as a coplanar waveguide inside the proposed antenna configuration. The ground component exhibits a distinct separation, but empirical evidence suggests that port 1 is interconnected with an SMA port. As a result, the ground terminal of port one is electrically linked to both the left and right ground planes of the monopole antenna's ground plane. Concurrently, the ground planes of port 2 and port 3 are associated with the adjacent left and right grounds, therefore establishing a transparent interconnection between all antenna ground planes [25]. The redesigned ground plane
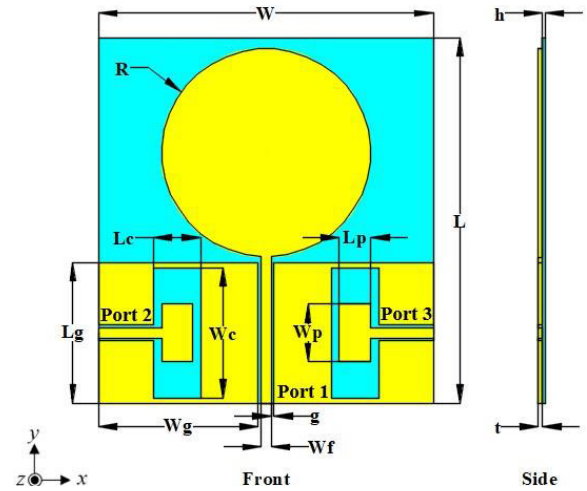

FIGURE 3. The proposed antenna configuration.

on both sides has been oriented parallel to the antenna feed in order to enhance antenna coupling. This results in the antenna being capable of resonating at a range of ultra-wideband frequencies.

The dimensions of the proposed antenna are established by (1) and (2), which ascertain the overall width (W) and length (L), respectively. The aforementioned metric is used to determine the comprehensive structural capability of the antenna, guaranteeing a minimum frequency response of 1.6 GHz.

$$W = \frac{c}{2f_r \left(\sqrt{\frac{\varepsilon_r + 1}{2}} \right)} \tag{1}$$

$$L = \frac{c}{2f_r \left(\sqrt{\varepsilon_{eff}} \right)} - 2\Delta L \tag{2}$$

Nevertheless, the UWB antenna has been specifically engineered to function at a resonant frequency falling between the ranges of 2.5 GHz to 10.6 GHz. The frequency range under consideration is established based on the vertical dimension of the circular monopole antenna. This dimension may be obtained by using (3), which is given as

$$R = \frac{c}{\left[4f_r \sqrt{\frac{\varepsilon_r + 1}{2}} \right]}. \tag{3}$$

Moreover, the design equation for the ultra-wideband (UWB) slot has been developed to handle a wide range of frequencies, including both low and high frequencies. The equation for determining the low frequencies may be represented as

$$f_L = \frac{c}{\left[2(W_c + L_c)\sqrt{\frac{\varepsilon_r + 1}{2}} \right]}, \tag{4}$$

where c represents the speed of light, W_c denotes the width of the conductor, L_c represents the length of the conductor,

TABLE 1. Parameter of proposed UWB MIMO antenna.

Parameter	Size (mm)	Parameter	Size (mm)
W	64	L	70
W_p	11	L_p	6
W_c	25	L_c	9
W_g	30.5	L_g	27
W_f	2	R	20
g	0.5	h	0.056
t	0.07		

and ε_r represents the relative permittivity. The equation representing high frequency may be mathematically represented as

$$f_H = \frac{c}{\left[4(W_c + L_c)\sqrt{\frac{\varepsilon_r+1}{2}} \right]}. \tag{5}$$

The designated frequency f_L is estimated to be about 3 GHz, while the designated frequency f_H is estimated to be around 9 GHz. Table 1 summarizes the fundamental parameters of the proposed antenna.

Then, the characteristics of the antenna structure will be evaluated, and the influence of the resonant frequency range will be explored. The height of a monopole antenna is contingent upon the radius parameter R of the antenna. As the value of the R parameter increases, there is a corresponding increase in the height of the antenna. Hence, the resonant frequency that impacts this parameter has been shifted toward the lower end. Consequently, the dimensions of the circular patch can be determined using (3). Figs. 4 displays the analysis of this phenomenon.

Fig. 4(a) illustrates the consequences of changing the parameter of R values relative to the $|S_{11}|$ level. Due to the increased electrical length of the radiator, raising the parameter of R concurrently shifted the resonant frequency range from 2 GHz to 12 GHz to the left. The impedance bandwidth between 2 GHz and 12 GHz fluctuates simultaneously. The magnitude change of the R parameter's height does not affect $|S_{22}|$ and $|S_{23}|$. This is because the wave reflection at Port 2 and Port 3 is not significantly impacted by the radius of the monopole antenna of Port 1. Furthermore, upon analyzing the electrical coupling between ports 1 to 2, ports 1 to 3, and ports 2 to 3 as illustrated in Fig. 4(b), it has been observed that the electrical coupling impact of ports 1 to 2 and ports 1 to 3 remains unchanged even upon increasing the R parameter. Minor variations in $|S_{21}|$ or $|S_{31}|$ at 6 GHz may occur as a result of electric fields produced by the under-arc region of the circular patch and the shared ground of the rectangular slot at ports 2 or 3. Furthermore, the absolute value of $|S_{32}|$ has minimal impact on the increase of the R parameter.

The results of the analysis of the reflection coefficients of $|S_{22}|$ and $|S_{33}|$ are illustrated in Fig. 5. It has been observed that an increase in the parameter W_p results in a decrease in
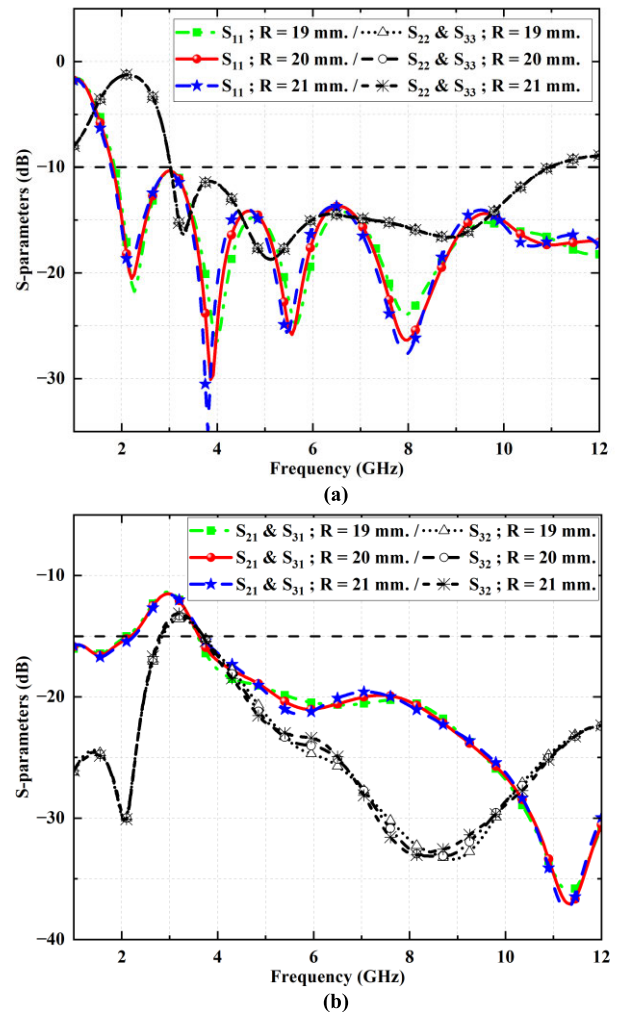

FIGURE 4. The simulation of the antenna characteristic as changing parameters R of (a) reflection coefficient of $|S_{11}|$, $|S_{22}|$, and $|S_{33}|$ and (b) insertion coefficient of $|S_{21}|$, $|S_{31}|$, and $|S_{32}|$.

the resonant frequencies of $|S_{22}|$ and $|S_{33}|$. This is attributed to the increased electrical length in the rectangular patch at port 2 and port 3. Based on the findings, it is recommended that the optimal parameter W_p be set to 9.0 mm in order to effectively cover the UWB bands. However, an increase in the W_p parameter did not result in any significant changes in $|S_{11}|$, $|S_{21}|$, $|S_{31}|$, and $|S_{32}|$. It is apparent that the W_p parameter has a significant impact on the impedance bandwidth of $|S_{22}|$ and $|S_{33}|$, particularly at high frequencies.

The impedance bandwidth effect resulting from the alteration of the L_p parameter is illustrated in Fig. 6(a). The rise in L_p produces a modification in the impedance bandwidth at a lower frequency of approximately 3.8 GHz, wherein the magnitudes of $|S_{22}|$ and $|S_{33}|$ experience a decline at this particular frequency. In contrast, the impact of the impedance bandwidth of $|S_{22}|$ and $|S_{33}|$ remained relatively stable across other frequency ranges. Furthermore, the magnitude of $|S_{11}|$ remains unaffected by a substantial variation in impedance
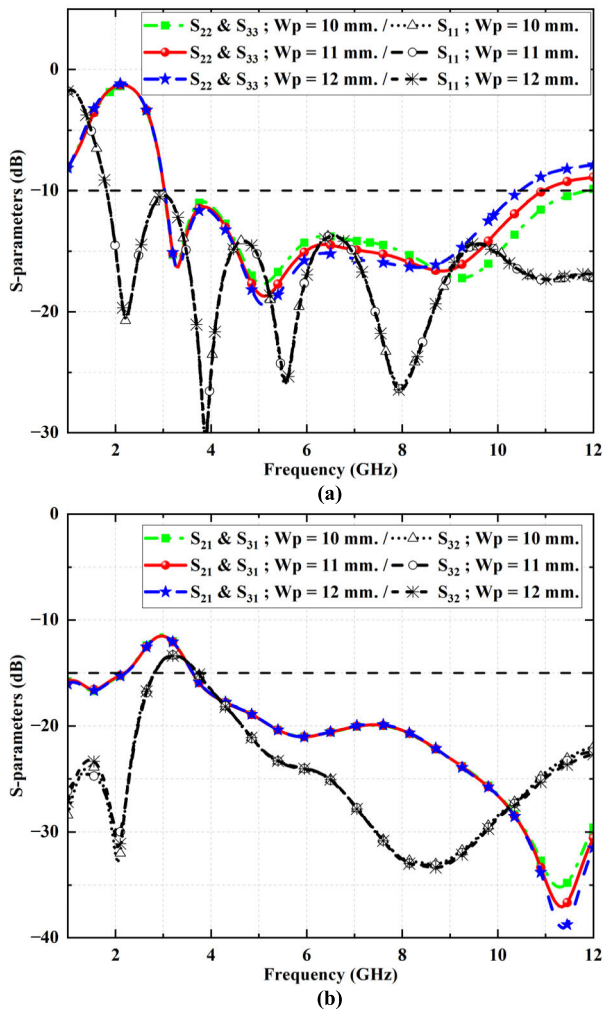
FIGURE 5. The simulation of the antenna characteristic as changing parameters W_p of (a) reflection coefficient of $|S_{11}|$, $|S_{22}|$, and $|S_{33}|$ and (b) insertion coefficient of $|S_{21}|$, $|S_{31}|$, and $|S_{32}|$.

FIGURE 6. The simulation of the antenna characteristic as changing parameters L_p of (a) reflection coefficient of $|S_{11}|$, $|S_{22}|$, and $|S_{33}|$ and (b) insertion coefficient of $|S_{21}|$, $|S_{31}|$, and $|S_{32}|$.

bandwidth throughout the entire frequency range of operation. Fig. 6(b) displays the simulation outcomes pertaining to the impacts of $|S_{21}|$, $|S_{31}|$, and $|S_{32}|$. The study revealed a positive correlation between the L_p parameter and the magnitude of $|S_{21}|$, $|S_{31}|$, and $|S_{32}|$ within the frequency range of 4 GHz to 12 GHz. The observed effect indicates that the L_p parameter has a significant impact on the electrical coupling between the ports of Port 1, Port 2, and Port 3.

The impact of the reflection coefficient and transmission coefficient on the W_c parameter alteration is illustrated in Figs. 7. The study revealed that an increase in the W_c parameter resulted in a decrease in the resonant frequencies $|S_{22}|$ at Port 2 and $|S_{33}|$ at Port 3, while $|S_{11}|$ at Port 1 remained unaffected. Simultaneously, upon increasing the W_c parameter and taking into account the transmission effect between Port 1, Port 2, and Port 3, it was observed that the resonant frequencies of $|S_{21}|$, $|S_{31}|$, and $|S_{32}|$ exhibited a significant decrease. An increase in the W_c parameter will result in an
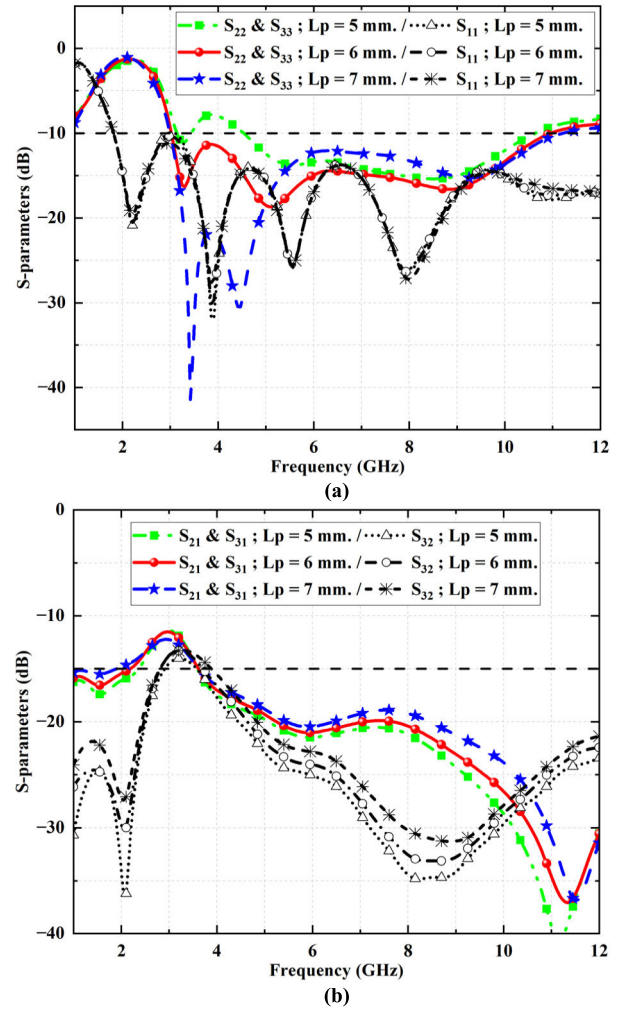
extension in the electrical length of the square patch in the slot, thereby causing a reduction in frequency.

Fig. 8(a) depicts the impact of altering the L_c parameter on the impedance bandwidth effect. An increase in L_c results in an adjustment of the impedance bandwidth at a lower frequency of around 3.8 GHz. At this specific frequency, the magnitudes of $|S_{22}|$ and $|S_{33}|$ undergo an increment. On the contrary, there is a reduction in the influence level of $|S_{22}|$ and $|S_{33}|$ over the frequency intervals ranging from 6 GHz to 9 GHz. Moreover, the magnitude of $|S_{11}|$ remains unchanged despite a significant fluctuation in impedance bandwidth across the complete frequency spectrum of operation. Fig. 8(b) illustrates the simulation results regarding the effects of $|S_{21}|$, $|S_{31}|$, and $|S_{32}|$. According to the study, it was observed that the values of $|S_{21}|$, $|S_{31}|$, and $|S_{32}|$ exhibit a decrease in magnitude with an increase in the L_c parameter, within the frequency range spanning from 4 GHz to 12 GHz. The results suggest that the L_c
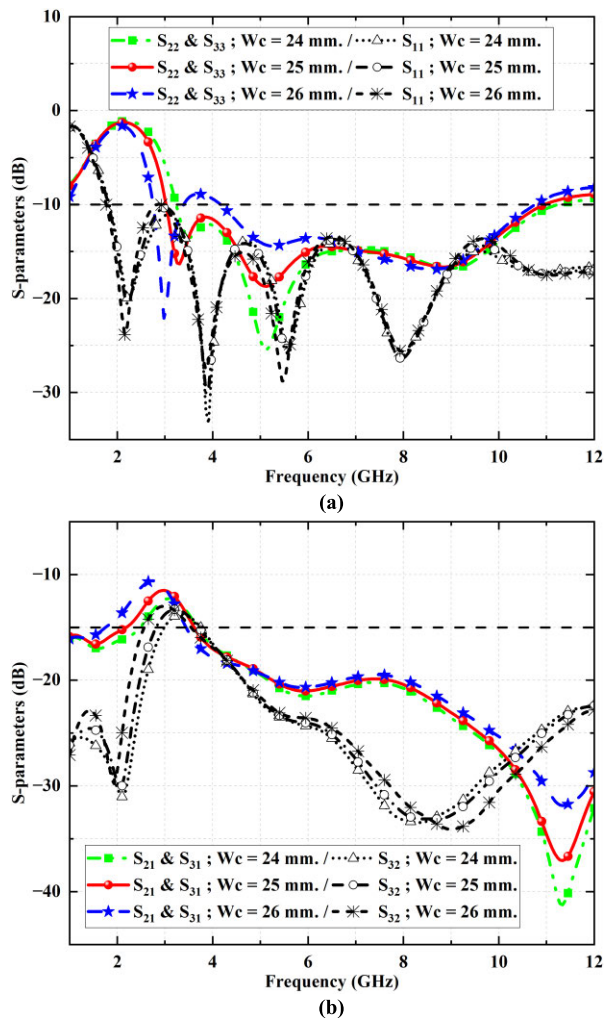
FIGURE 7. The simulation of the antenna characteristic as changing parameters W_c of (a) reflection coefficient of $|S_{11}|$, $|S_{22}|$, and $|S_{33}|$ and (b) insertion coefficient of $|S_{21}|$, $|S_{31}|$, and $|S_{32}|$.
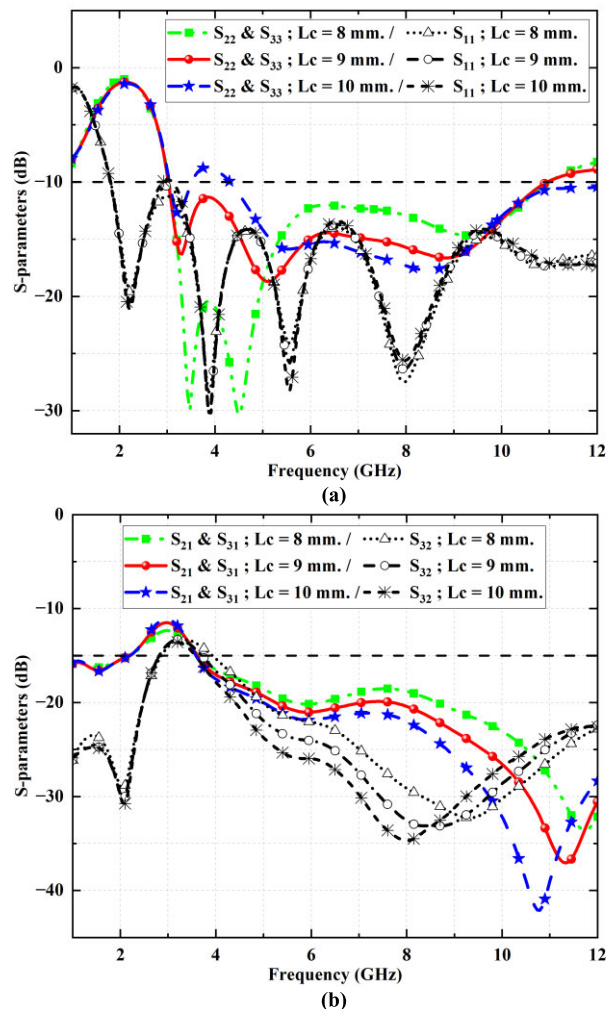

FIGURE 8. The simulation of the antenna characteristic as changing parameters L_c of (a) reflection coefficient of $|S_{11}|$, $|S_{22}|$, and $|S_{33}|$ and (b) insertion coefficient of $|S_{21}|$, $|S_{31}|$, and $|S_{32}|$.

parameter contributes a crucial role in the electrical coupling among the ports of Port 1, Port 2, and Port 3. This is attributed to the electrical coupling between the circular patch and the ground slot.

The reflection coefficient is not a comprehensive indicator of the radiation efficiency and bandwidth of a MIMO antenna. The total active reflection coefficient (TARC or Γ^t), which takes into account both coupling and random signal combination, may be utilized in place of the basic reflection coefficient. TARC offers a more accurate way to quantify MIMO effectiveness as a result. In the context of port excitation, it is customary to consider the summation of power accessible at all excitation ports as the incident power (P_{inc}). The power that is radiated is then regarded as the transferred power (P_{rad}), while the discrepancy between these two quantities is referred to as the reflected power (P_{ref}). The TARC is technically defined as the square root of the ratio between the reflected power (P_{ref}) and the incident

power (P_{inc}), as denoted by (6), [26].

$$\Gamma^t = \sqrt{\frac{P_{ref}}{P_{inc}}} = \sqrt{\frac{P_{inc} - P_{rad}}{P_{inc}}} \tag{6}$$

The TARC for a lossless N-port antenna may be determined using (7) as shown in [27].

$$\Gamma^t = \sqrt{\frac{\sum\limits_{i=1}^{N} |b_i|^2}{\sum\limits_{i=1}^{N} |a_i|^2}} \tag{7}$$

Typically, TARC values are represented as real numbers within the range of $0 \leq \text{TARC} \leq 1$. If the TARC is equal to zero, the whole of the power is effectively sent to the antenna. Conversely, if the TARC is equal to one, the complete power is either reflected to the antenna at the same port or redirected to another port where another antenna is located. This paper utilizes the TARC value to assess the performance of specific
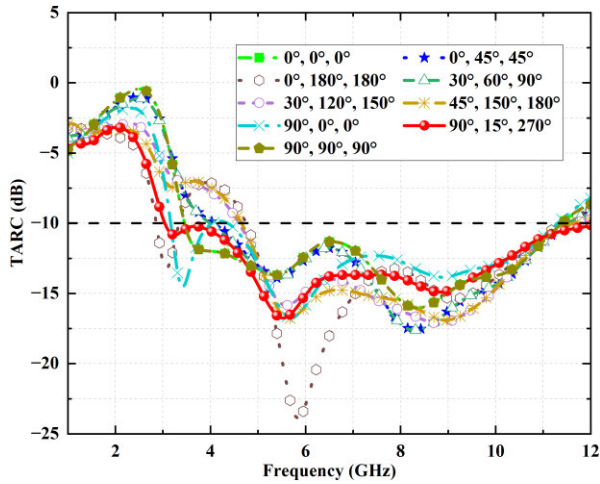
FIGURE 9. TARC results of the proposed UWB MIMO antenna as altering the theta phase angles at port 1, port 2, and port 3.

FIGURE 10. MEG results of the proposed UWB MIMO antenna with XPR =0 dB and 6 dB at port 1, port 2, and port 3.

antennas and ports by comparing them with varying excitation at various theta phase angles. Figure 9 illustrates that the TARC values acquired exhibited a consistent trend of being below -10 dB over the full frequency spectrum of 3 GHz - 11 GHz, across different theta phase angles. The theta phase angles that yielded the lowest TARC value were determined to be 90, 15, and 270 degrees at port 1, port 2, and port 3, respectively. According to the results, the findings indicate that the excitation of the incident signal at varying angles in each port leads to fluctuations in TARC. Nevertheless, the variation in bandwidth resulting from differing excitation angles has little impact on the low-frequency range. Another diversity measure called mean effective gain (MEG) may be used to assess the wireless channel characteristics. The quantity under consideration is the ratio of the average received power (P_{rec}) to the overall average incident power (P_{inc}). The equation for the MEG is represented by equations (8) and (9) [28].

$$MEG_i = \frac{P_{rec}}{P_{inc}}$$
$$= \oint \left[\frac{XPR \cdot G_{\theta i}(\Omega) \cdot P_\theta(\Omega) + G_{\phi i}(\Omega) \cdot P_\phi(\Omega)}{1 + XPR} \right] d\Omega \quad (8)$$

or

$$MEG_i = \int_0^{2\pi} \int_0^\pi \left[\frac{\frac{XPR}{1+XPR} G_\theta(\theta, \phi) P_\theta(\theta, \phi)}{+ \frac{1}{1+XPR} G_\phi(\theta, \phi) P_\phi(\theta, \phi)} \right] \sin\theta \, d\theta \, d\phi \quad (9)$$

The angular density functions of incoming power are denoted as P_θ and P_φ, whereas the gain functions are represented by G_θ and G_φ.

In this research, the determination of the MEG value is conducted by the use of the CST simulation program. The determination of the MEG entails the use of the
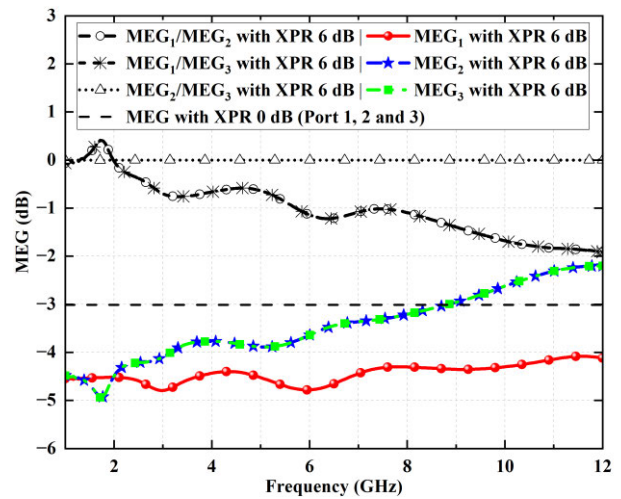
cross-polarization ratio (*XPR*) inside the far-field region. Isotropic antennas were used to compute MEG, exhibiting *XPR* values of 0 dB and 6 dB, correspondingly. In order to achieve maximum diversity gain, it is essential to maintain a near unity ratio for the MEG between the two antennas. This guarantees that the received power by each antenna is about equal on average. According to the data shown in Figure 10, there is evidence suggesting a positive association between the influence of MEG_1 and frequency. Additionally, MEG_2 and MEG_3 reveal a significant positive relationship with frequency. As a result, the MEG ratio between MEG_1 and MEG_2, as well as between MEG_1 and MEG_3, exhibits a significant decline over the whole spectrum of operating frequencies. However, it is important to note that the observed decrease in values was within the acceptable range of around ±3 dB, as shown by citations [29] and [30]. Furthermore, it is evident that the MEG ratio between MEG_2 and MEG_3 stays consistent at 0 dB throughout the whole spectrum of operating frequencies. This observation illustrates the significant diversity gain shown by the MIMO antenna under consideration.

The CST simulation program will be utilized to evaluate the current dissolution. The suggested antenna's current distribution in each port is shown in Figs. 11-13 based on simulation findings. Figs. 11 displays the current distribution on a monopole antenna. It is evident that the predominant current flow is concentrated within the circular patch region. The resonant frequencies that occur are determined by the height of the circular patch. It is obvious that during the simulation of operations at higher frequencies, the current level is observed at the lower end of the patch circle. It is noteworthy that the alteration in the size of the patch circle will impact the resonant frequency that was previously tested by modifying the *R* parameter. Furthermore, the quantity of current was identified at the upper ground edge, which
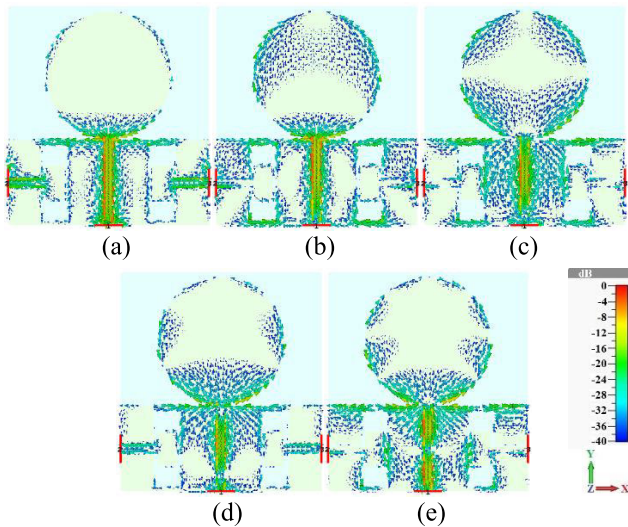
FIGURE 11. The current distribution of the proposed UWB MIMO antenna Port 1 at the frequency of (a) 2.45 GHz, (b) 3.5 GHz, (c) 5.5 GHz, (d) 7 GHz, and (e) 10 GHz.
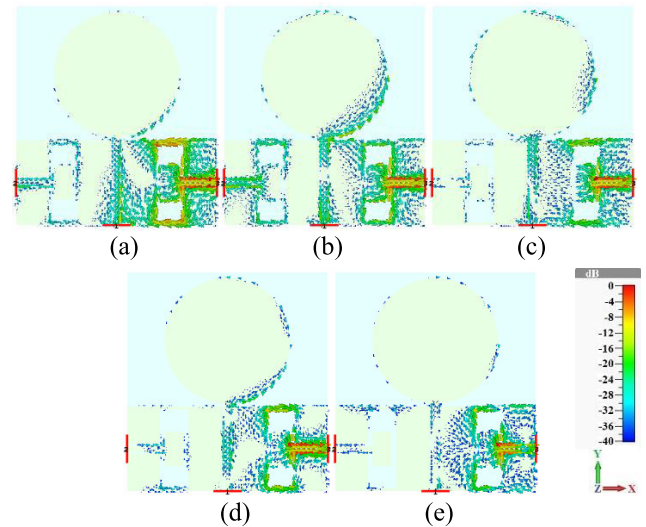

FIGURE 13. The current distribution of the proposed UWB MIMO antenna Port 3 at the frequency of (a) 2.45 GHz, (b) 3.5 GHz, (c) 5.5 GHz, (d) 7 GHz, and (e) 10 GHz.
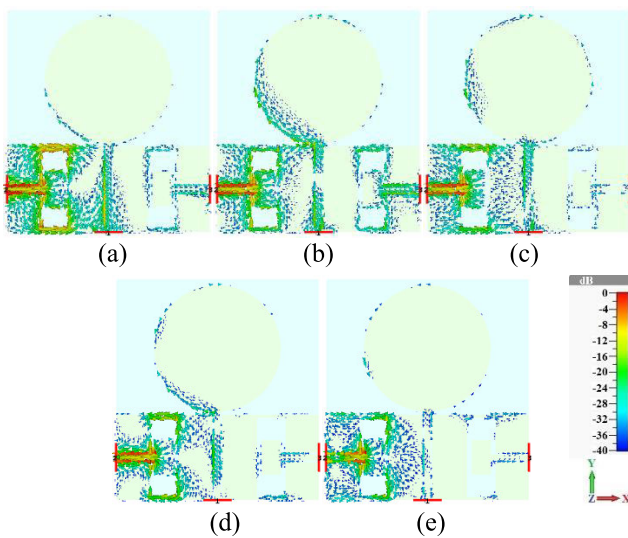

FIGURE 12. The current distribution of the proposed UWB MIMO antenna Port 2 at the frequency of (a) 2.45 GHz, (b) 3.5 GHz, (c) 5.5 GHz, (d) 7 GHz, and (e) 10 GHz.

FIGURE 14. The prototype structure of the proposed UWB MIMO antenna.

corresponds to the L_c parameter that influenced the alteration in transmission coefficients of $|S_{21}|$ and $|S_{31}|$.

The current distribution results of the proposed antenna at port 2 and port 3 are depicted in Figs. 12 and 13, respectively. The analysis indicates a significant current distribution in the upper ground edge of the L_c parameter across all resonant frequency ranges of the antenna. This finding is in accordance with previous simulation results, which demonstrate the substantial impact of the L_c parameter on the reflection coefficient and transmission coefficient of the antenna throughout its operating frequency range. Furthermore, the low-frequency range exhibits a substantial current on the ground edge of parameter W_c. The current magnitude at

high frequency seems significant in the rectangular patch region within the slot that corresponds to the W_p parameter. The analysis indicates that the inner slot length of the W_c parameter is impacted at low frequencies, whereas the rectangular patch length of the W_p parameter has an effect at high frequencies. This finding is consistent with the previously reviewed parametric transformation study.

Based on previous research on the impact of alterations to different parameters. The prototype antenna was constructed using optimal parameters, as depicted in Fig. 14. The subsequent section will delve into additional information regarding the construction and measurement procedures utilized.

III. RESULT AND DISCUSSIONS
A. ULTRA-WIDEBAND MIMO ANTENNA RESULT
A prototype UWB MIMO antenna was manufactured by slicing a carbon black thin film for a monopole antenna substrate
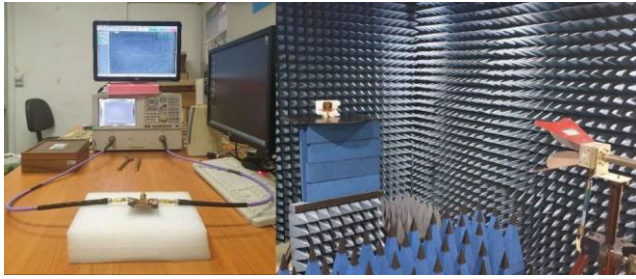
FIGURE 15. Experimental setup for measuring the characteristics and efficiency of the proposed antenna.

from a $64 \times 70 \times 0.056$ mm3 film base material using scissors and a cutter. The sliced film was then attached to a copper tape antenna measuring $64 \times 70 \times 0.07$ mm^3. The CPW feed is utilized to establish a connection between the antennas and a 50Ω SMA connector, as illustrated in Fig. 14. Furthermore, film-based antennas possess the characteristic of being bendable and flexible, thereby enabling their application in curved regions of an automobile. Subsequently, utilize the network analyzer to perform experiments on the prototype antenna in order to assess its characteristics and efficacy, employing the Agilent model E8363B as illustrated in Fig. 15. The frequency range of the proposed antenna under consideration was determined through experimentation with its reflection coefficient. Fig. 16 depicts the simulated and measured reflection coefficients of the proposed antenna, specifically $|S_{11}|$, $|S_{22}|$, and $|S_{33}|$. Based on the findings of $|S_{11}|$, it has been determined that the proposed antenna's simulated and measured results are functional within the frequency range of 1.9 GHz to 12 GHz. Similarly, the simulated and measured results of $|S_{22}|$ and $|S_{33}|$ indicate that they operate effectively within the frequency range of 3 GHz to 11 GHz. This indicates that the proposed antenna under consideration exhibits responsiveness on three ports, with a reflection coefficient that is lower than -10 dB. Thus, it is suggested that the proposed antenna has the capability to cover the ultra-wideband spectrum ranging from 3.1 GHz to 10.6 GHz (FCC) and facilitate WPAN applications. Furthermore, the experiment conducted to determine the transmission coefficient isolation among triple ports involves measuring $|S_{21}|$, $|S_{31}|$, and $|S_{23}|$, which correspond to port 1 (the first antenna), port 2 (the second antenna), and port 3 (the third antenna), respectively. The transmission coefficients of $|S_{21}|$, $|S_{31}|$, and $|S_{32}|$ are depicted in Fig. 17, both in simulated and measured forms. Research findings indicate that the transmission coefficients of the proposed UWB MIMO antenna do not exceed -12 dB. Based on the findings, it can be concluded that the proposed antenna exhibits a transmission coefficient of less than -12 dB within the frequency range of 3 GHz to 12 GHz. This indicates that the triple port antennas operate independently across the aforementioned frequency range. Furthermore, the results obtained from the simulation and measurement were in agreement. The minor discrepancy observed could potentially be attributed to the formation between the feed
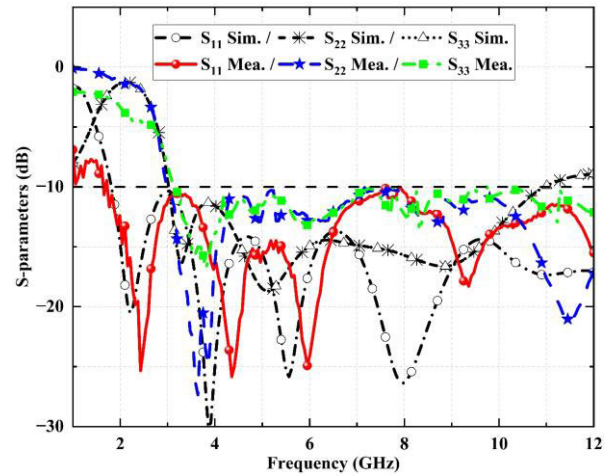

FIGURE 16. Simulated and measured result of the $|S_{11}|$, $|S_{22}|$ and $|S_{33}|$ of the proposed antenna.
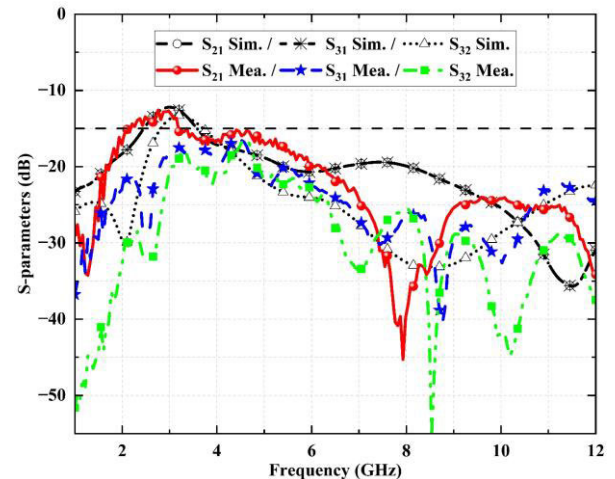

FIGURE 17. Simulated and measured result of the $|S_{21}|$, $|S_{31}|$ and $|S_{32}|$ of the proposed antenna.

line and the radiator, as well as the gap present between the transmission line and the ground plane.

According to the results shown in Fig. 18, it can be seen that the antenna efficiency exceeds 85% in the frequency range spanning from 4 GHz to 12 GHz for all three ports. In the lower frequency range of less than 4 GHz, the efficiency of the antenna is seen to be below 85% due to the power loss associated with the antenna. Consequently, it is not possible to establish the precise Envelope Correlation Coefficient (ECC) within the frequency range of 3 GHz -11 GHz only relying on the S-parameter.

The crucial parameter in the MIMO system is the separation between the antenna elements, according to the specifications of the MIMO antenna. The present study examines the Envelope Correlation Coefficient (ECC) of the UWB MIMO antenna. Nevertheless, in cases where there are losses inside the antenna system, it becomes imperative to assess
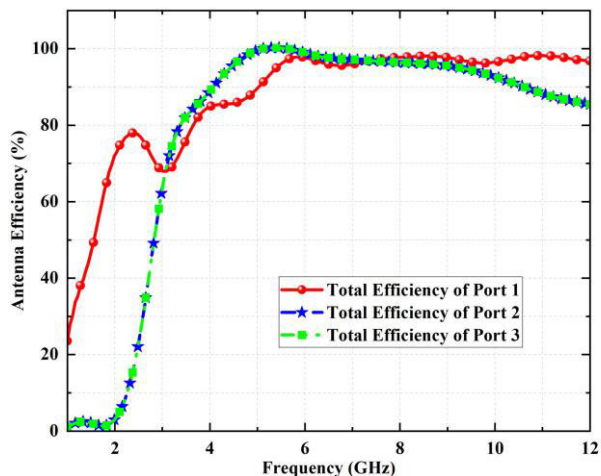
FIGURE 18. Simulated antenna efficiency of the port 1, port 2 and port 3 of the proposed antenna.

FIGURE 19. The correlation coefficient of the prototype UWB MIMO antenna.

the *ECC* values derived from the far-field characteristic [25]. This approach is preferred over relying only on *ECC* considerations based on S-parameters since it allows for more accuracy. The *ECC* has undergone modifications using the far-field computing method outlined in (10) to (12) and was analyzed by the simulation software CST:

$$ECC_{12} = \frac{\left|\iint\limits_{4\pi} [E_1(\theta, \phi) * E_2(\theta, \phi)]\, d\Omega\right|^2}{\iint\limits_{4\pi} |E_1(\theta, \phi)|^2\, d\Omega \iint\limits_{4\pi} |E_2(\theta, \phi)|^2\, d\Omega}, \quad (10)$$

$$ECC_{13} = \frac{\left|\iint\limits_{4\pi} [E_1(\theta, \phi) * E_3(\theta, \phi)]\, d\Omega\right|^2}{\iint\limits_{4\pi} |E_1(\theta, \phi)|^2\, d\Omega \iint\limits_{4\pi} |E_3(\theta, \phi)|^2\, d\Omega}, \quad (11)$$

$$ECC_{23} = \frac{\left|\iint\limits_{4\pi} [E_2(\theta, \phi) * E_3(\theta, \phi)]\, d\Omega\right|^2}{\iint\limits_{4\pi} |E_2(\theta, \phi)|^2\, d\Omega \iint\limits_{4\pi} |E_3(\theta, \phi)|^2\, d\Omega}, \quad (12)$$

where $E_i(\theta, \varphi)$ represents the complex three-dimensional pattern of the electric field produced by the antenna at port *i*.

The gain diversity values can be obtained by utilizing either the radiation patterns. Assuming a uniform multipath environment with a value below 0.5, the (10), (11), and (12) can be employed to calculate the *ECC*. Based on the findings presented in Fig. 19 of the *ECC*'s results, it has been determined that the *ECC* remains below 0.45 within the frequency range of 2 GHz to 12 GHz. This indicates that the prototype UWB MIMO antenna is capable of transmitting and receiving data utilizing multiple inputs and multiple outputs (MIMO) technology.

The peak gain of the proposed antenna at each port is depicted in Fig. 20, showing both the measured and simulated
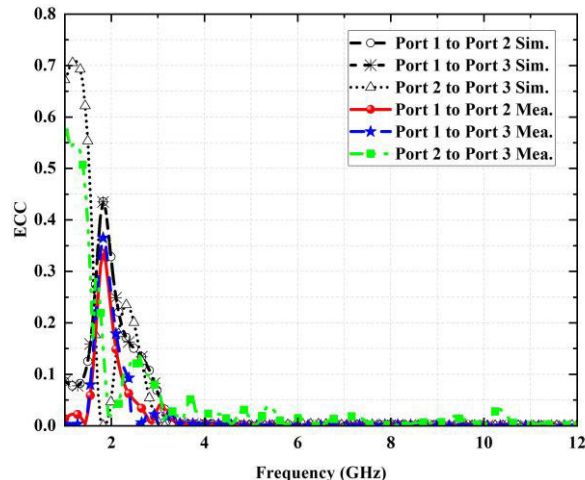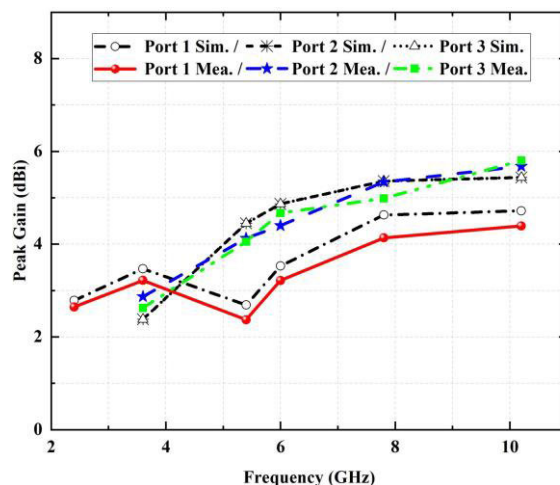

FIGURE 20. Comparison of the proposed antenna peak gain between simulated result and measured result.

results. The antenna's peak gains at port 1 range from 3.6 dBi between 2 GHz to 11 GHz, with the exception of 5.4 GHz where it is approximately 2.3 dBi. Furthermore, the antenna's peak gains observed at ports 2 and 3 exhibit values exceeding 5 dBi within the frequency range of 5 GHz to 11 GHz, whereas they demonstrate values of approximately 3 dBi within the frequency range of 2 GHz to 5 GHz. The antenna's peak gains at ports 2 and 3 will offset the low gain impact at port 1 at 6 GHz in the event that the signal from the first antenna experiences a weak signal. This represents a notable advantage of the MIMO antenna design in question. Similarly, a comparison between simulation and measurement results demonstrates a high level of concurrence.

Due to the varied resonance frequencies that UWB antennas are responsive to, it is imperative to maintain a low group delay to mitigate any phase distortion issues that may arise from electromagnetic waves interacting with the antenna
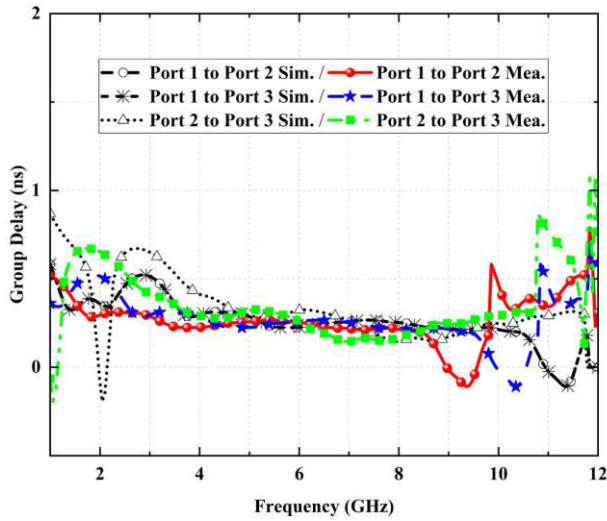
FIGURE 21. The group delay of the prototype UWB MIMO antenna.

across multiple wavelength dimensions. The group delay of the antenna under consideration has been evaluated by utilizing two UWB antennas positioned at a distance of 1 meter from each other in a front-to-front configuration.

Fig. 21 depicts the group delay outcomes of the proposed antenna. It is evident that for practical bandwidths ranging from 3 GHz to 11 GHz, the variation in ground delay is less than 0.85 ns. The proposed antenna exhibited minimal distortion in the UWB pulse shape due to its activation by a short pulse.

As seen in Figs. 22, 23, and 24, the propagation patterns of the proposed antenna are evaluated at each port of 1, 2, and 3, respectively. Fig. 22 depicts the *X-Z* and *Y-Z* radiation patterns of the proposed antenna at the first port. The antenna under consideration exhibits omnidirectional radiation patterns at frequencies of 2.4 GHz, 3.6 GHz, 5.4 GHz, and 6 GHz. However, at higher frequencies of 7.8 GHz and 10.2 GHz, the radiation patterns deviate from the conventional omnidirectional pattern due to the higher-order mode. Moreover, the cross-polarized extension was observed on the *X-Z* and *Y-Z* planes with an increase in frequency. Figs. 23 and 24 display, respectively, the radiation patterns resulting from the development of the slot antenna on the ground plane at ports 2 and 3. The directional characteristics of the proposed antenna have been analyzed and it has been observed that the radiation patterns of the proposed antenna are bidirectional at 5.4 GHz, 6 GHz, 7.8 GHz, and 10.2 GHz on the *X-Z* and *Y-Z* planes. However, at 3.6 GHz, the radiation pattern exhibits slight variations due to the low coupling effect between ports 1 and 2, as well as between ports 1 and 3, as evidenced by the $|S_{21}|$ and $|S_{31}|$ measurements. Based on the obtained measurements, it was seen that the propagation pattern exhibited instability over the whole operating frequency range. This instability may be attributed to the
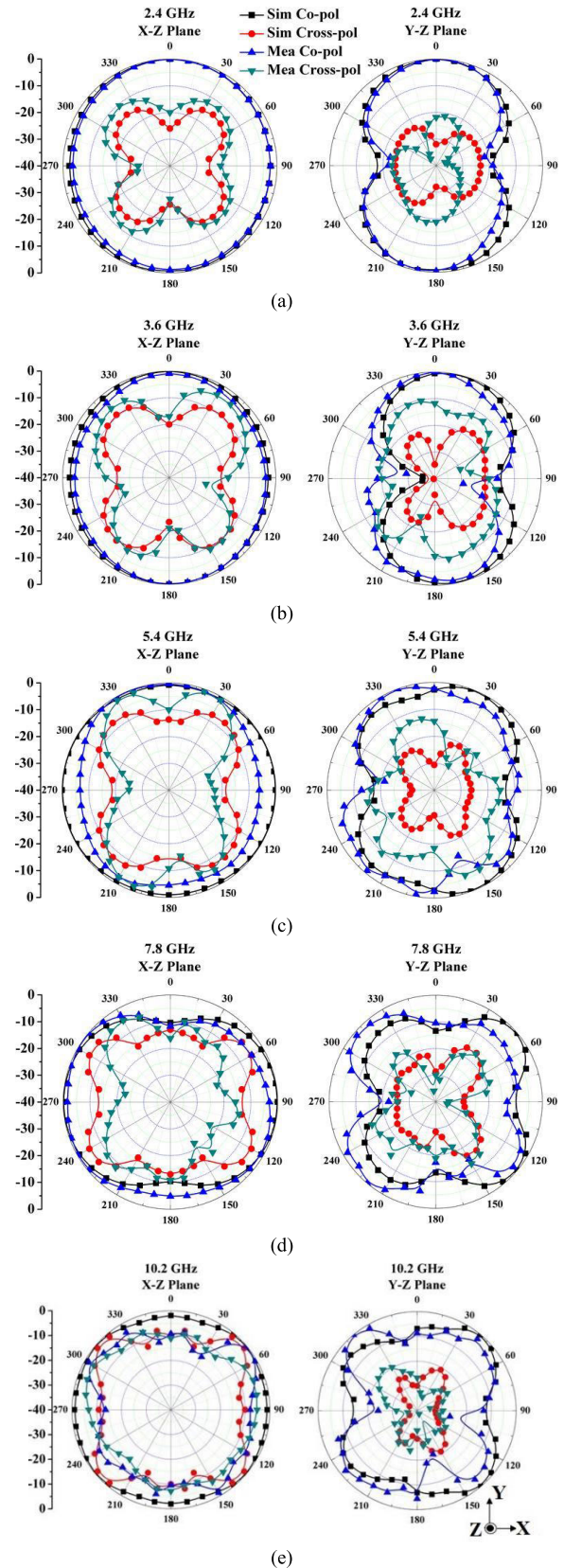

FIGURE 22. Radiation pattern comparisons of prototype UWB MIMO antennas for Port 1 at (a) 2.4 GHz, (b) 3.6 GHz, (c) 5.4 GHz, (d) 7.8 GHz, and (e) 10.2 GHz.

FIGURE 23. Radiation pattern comparisons of prototype UWB MIMO antennas for Port 2 at (a) 3.6 GHz, (b) 5.4 GHz, (c) 6 GHz, (d) 7.8 GHz, and (e) 10.2 GHz.

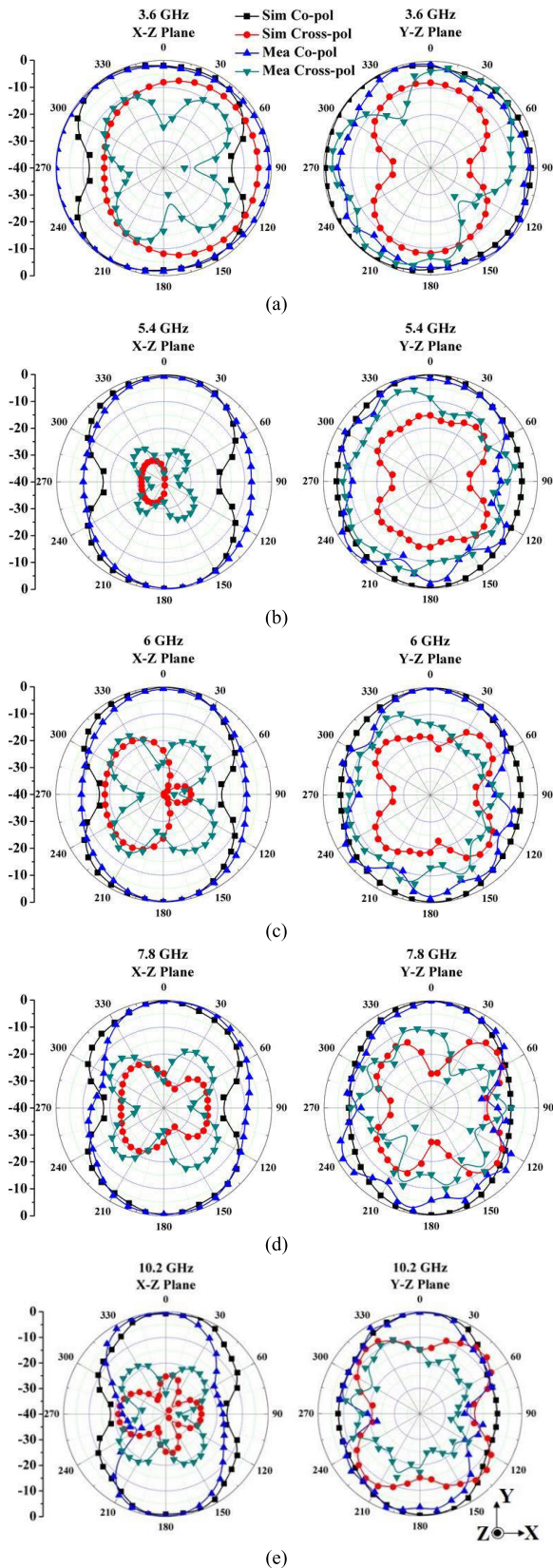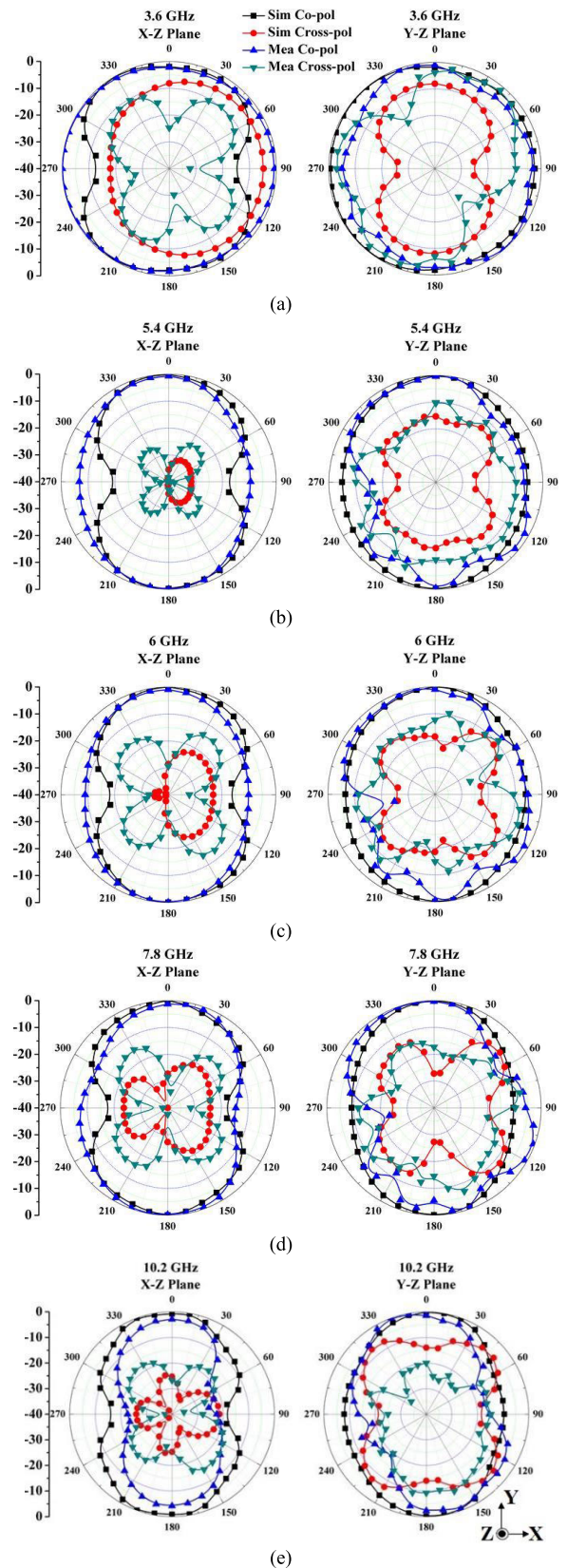**FIGURE 24.** Radiation pattern comparisons of prototype UWB MIMO antennas for Port 3 at (a) 3.6 GHz, (b) 5.4 GHz, (c) 6 GHz, (d) 7.8 GHz, and (e) 10.2 GHz.

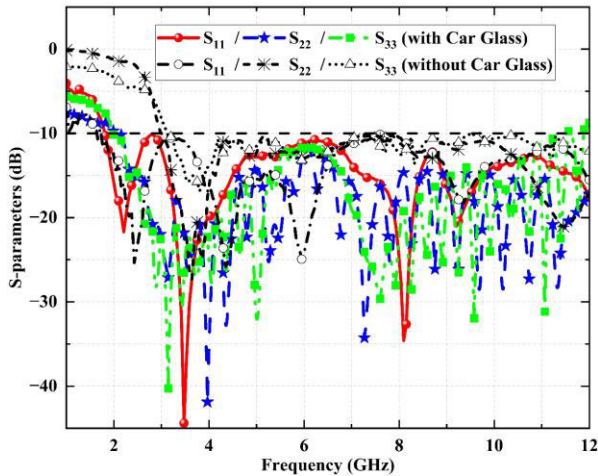**FIGURE 25.** Performing measurements on the antenna's characteristics as installed on the windshield.

FIGURE 26. Comparison of the antenna reflection coefficient of each port when installed on the windshield.

FIGURE 27. Comparison of the antenna transmission coefficient of each port when installed on the windshield.
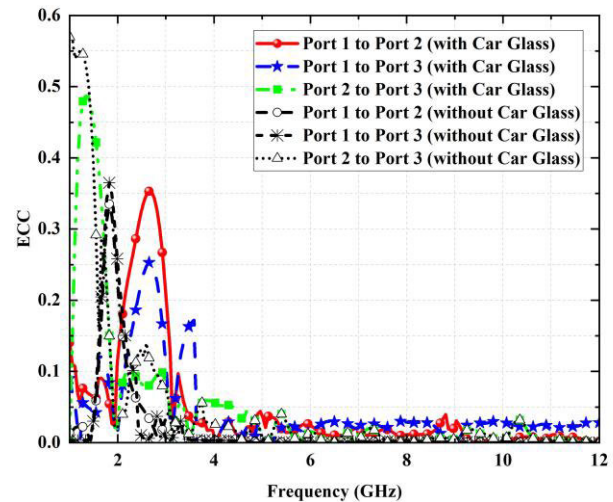
FIGURE 28. The correlation coefficient of the prototype UWB MIMO antenna installed on the windshield.

presence of higher-order modes in the antenna. Notably, when the harmonic frequency was raised, the propagation pattern became deformed. Nevertheless, the antenna under consideration remains capable of fulfilling the practical requirements as previously stated.

The test results presented in Fig. 25 depict the effect measurement of the proposed antenna when used in conjunction with a windshield mount. The purpose of the test was to analyze the impact of the reflection coefficient and transmission coefficient on each port. The properties of the proposed antenna when mounted together with the windshield were measured, and the results are shown in Fig. 26. It has been observed that there was a slight reduction in the magnitude of the reflection coefficient in each port of $|S_{11}|$, $|S_{22}|$, $|S_{33}|$. However, there was almost no significant change observed in the impedance bandwidth. Consequently, the antenna under consideration is capable of operating within the frequency range of 3 GHz-11 GHz. The transmission coefficient of the antenna in each port, when installed with the windshield, is depicted in Fig. 27. It has been observed that the magnitudes of $|S_{21}|$ and $|S_{31}|$ have exhibited a slight decrease, whereas the magnitude of $|S_{32}|$ has shown a noticeable reduction within the frequency ranges of 3 GHz – 6 GHz
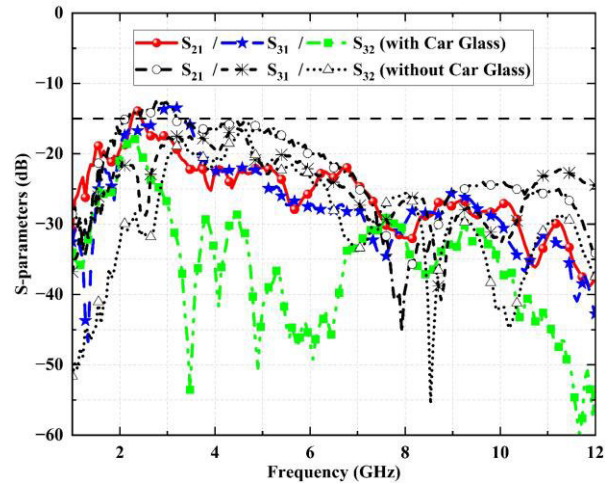
and 10 GHz – 12 GHz. The reason for this phenomenon is that the dielectric constant of the vehicle exceeds that of the car film. Consequently, the antenna's overall dielectric constant increases when installed on the windshield, leading to a modification in the impedance bandwidth on $|S_{11}|$, $|S_{22}|$, $|S_{33}|$, $|S_{21}|$, $|S_{31}|$, and $|S_{32}|$. Additionally, the antenna under consideration exhibits the ability to function within the frequency range of 3 GHz to 11 GHz, rendering it suitable for employment in a variety of wireless communication systems such as Ultra-Wideband (UWB), Fifth Generation (5G), Wireless Local Area Network (WLAN), Worldwide Interoperability for Microwave Access (WiMAX), and Wireless Personal Area Network (WPAN).

The *ECC* value can be computed from the measured radiation pattern value of the far field, which was acquired through the installation of the antenna on the windshield. This can be achieved by applying (10) to (12), as illustrated in

TABLE 2. Performance comparison of the proposed antenna with previously published literature.

Ref	Dimension (mm.), (Volume) (mm³)	Antenna, (Number of Element)	Substate (εr)	App.	Freq. Band (GHz), (%BW)	Ant Eff., ECC	Pol.	Gain (dBi)
[31]	90×90×2.5 (20,250)	1×1 (1)	TCFs (2.5)	Telemetry, Tracking & Command	2.025-2.11 (4.11%), 2.2-2.29 (27.45%)	72.3%, -	Linear	5.31
[32]	28×17×0.254 (121)	1×4 (4)	Rogers 5880 (2.2)	Radar detection & Sign monitoring	91-108 (17%)	82%, -	Linear	11.7
[33]	45×24×4 (4,320)	1×1 (1)	RTV Silicone Rubber (3.5)	EM head imaging systems	0.45-3.6 (155.56%)	-, -	Circular	9.0
[34]	50×60×1.3 (3,900)	1×1 (1)	FPMC (2.7)	Automotive	-	75%, -	Circular	11.9
[35]	10×10×0.5 (50)	1×1 (1)	KNN Ferro-electric (9.8)	Tunable Microwave Device	15.22-15.97 (4.80%)	-, -	Circular	2.0
[36]	17×10×0.5 (85)	1×1 (1)	VO2 Films Embedded (2.9)	5G (Millimeter-wave)	27.7–29.8 (7.30%), 38.8-40 (3.04%), 21.1-21.6 (2.34%), 38.6–40 (3.56%)	75% & 95%, -	Linear	9.5
[37]	24×24×0.8 (461)	2×2 (4)	Roger 5880 (2.2)	5G (Millimeter-wave)	24.8-44.45 (79.35%)	85%, Farfeild	Linear (Dual)	8.6
[38]	150×75×0.8 (9,000)	4×2 (8)	FR-4 (4.4)	Smart phones	3.3-6.0 (58%)	75%, Farfeild	Linear (Dual)	4.4
[39]	150×75×0.8 (9,000)	4×2 (8)	FR-4 (4.4)	Smart phones	3.3-8.5 (88%)	75%, S-Par.	Linear (Dual)	6.0
[40]	13×25×0.254 (83)	2×1 (2)	Roger 5880 (2.2)	Smart phones	2-12 (142.86%)	-, S-Par.	Linear	4.8
[41]	50×35×1.59 (2,783)	2×1 (2)	Jeans (1.6)	Textile	1.83-13.82 (153.20%)	85%, S-Par.	Linear	4.21
Proposed Ant.	64×70×0.126 (565)	3×1 (3)	Black Carbon Films (3.2)	Automotive	2-12 (142.86%)	85%, Farfeild	Linear (Dual)	5.8

Fig. 28. Based on the aforementioned findings, it has been determined that the *ECC* value remained consistently below 0.45 throughout the frequency range of 2 GHz to 12 GHz. The antenna under consideration demonstrates consistent transmitting and receiving capabilities in the context of multiple-input, multiple-output (MIMO) technology.

Additionally, following an evaluation of the antenna mounted to the windshield for the purpose of ascertaining its group delay, it was noted that the group delay of the windshield-installed antenna was greater in comparison to the antenna installed without the windshield. This was attributed to the higher dielectric constant of the windshield. Nonetheless, it is noteworthy that the group delay within the frequency spectrum of 3 GHz to 11 GHz remains below 2 ns, as depicted in Fig. 29. The results indicate that the antenna under consideration demonstrates minimal distortion in the shape of the
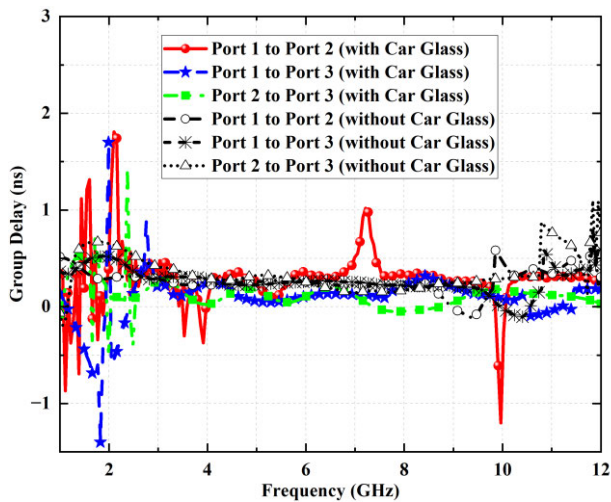
FIGURE 29. The group delay of the prototype UWB MIMO antenna installed on the windshield.

ultra-wideband pulse upon activation by a short pulse. Table 2 presents a comparison between the reference antenna and the proposed antenna.

Empirical evidence supports that the black carbon automotive film-based UWB MIMO antenna exhibits a greater fractional bandwidth and slimmer profile in comparison to the reference antenna. The antenna under consideration prioritizes characteristics such as slimness, pliability, and cost-effectiveness. When comparing the reference work to the present research, it can be seen that the antenna properties, including volume, flexibility, cost-effectiveness, and operating frequency spectrum, are within acceptable limits.

An advantageous characteristic of using black carbon films, a thin and flexible material, in the design of an antenna is its ability to be effectively affixed to curved surfaces, such as windshields, resulting in an aesthetically pleasing and harmonious appearance. Furthermore, it is worth noting that the antenna exhibits a significant percentage of bandwidth. However, it is important to recognize that the rigid and inflexible nature of FR4 makes it unsuitable for automotive windshield installations. Due to its inability to be flexed into a curved shape for attachment onto the windshield surface. Consequently, the aesthetic appeal of the product is lacking, and it fails to contribute to the economic growth of the automotive sector.

Therefore, based on previous antenna qualification tests, it has been determined that the proposed antenna is capable of detecting frequencies within the range of 3 GHz to 11 GHz. Consequently, this antenna exhibits potential for implementation in various wireless communication systems, including but not limited to UWB, WLAN, WiMAX, WPAN, and 5G applications.

IV. CONCLUSION

This paper presents a novel triple port UWB MIMO antenna that utilizes a flexible thin film for various wireless applica-

tions such as UWB, WLAN, WiMAX, WPAN, and 5G. The proposed antenna employed a carbon black window film as its substrate due to its thinness, affordability, and easy accessibility. To address the UWB range in the horizontal plane, modifications were made to the ground plane of the triple port antenna, resulting in the provision of slots on both sides of the antenna. The antenna's properties were analyzed using simulation software developed by CST. The antenna exhibits a bandwidth of approximately 142.86% (ranging from 2 GHz to 12 GHz) at port 1, while at ports 2 and 3, it demonstrates a bandwidth of 114.29% (ranging from 3 GHz to 11 GHz). The level of isolation exhibited by the radiator components of the antenna is below -12 dB. The antenna under consideration is capable of sustaining an average gain of over 5.8 dBi throughout its operation due to the radiating element of ports 2 and 3 compensating for the electromagnetic wave propagation of port 1 at a frequency of 6 GHz. Furthermore, the antenna's radiation pattern exhibits omnidirectional characteristics at port 1, while at ports 2 and 3, it displays bidirectional characteristics. According to the comparative outcomes presented in Table 2, the proposed antenna has the capability to achieve a high fractional bandwidth while maintaining a low profile. Furthermore, the implementation of a triple port ultra-wideband (UWB) multiple-input multiple-output (MIMO) antenna utilizing a flexible thin film substrate enables the feasibility of utilizing curved surfaces, as well as facilitating the integration of UWB, WLAN, WiMAX, WPAN, and 5G applications within MIMO systems.

REFERENCES

[1] B. P. Crow, I. Widjaja, J. G. Kim, and P. T. Sakai, "IEEE 802.11 wireless local area networks," *IEEE Commun. Mag.*, vol. 35, no. 9, pp. 116–126, Sep. 1997.

[2] D. V. Kumar, B. K. Mohan, and M. S. R. Shekar, "A person centered network concept: WPAN," *Asian J. Inf. Technol.*, vol. 4, no. 2, pp. 198–207, 2005.

[3] E. Pérez, R. Parada, and C. Monzo, "Global emergency system based on WPAN and LPWAN hybrid networks," *Sensors*, vol. 22, no. 20, pp. 1–20, Oct. 2022.

[4] S. A. Salehi, M. A. Razzaque, I. Tomeo-Reyes, and N. Hussain, "IEEE 802.15.6 standard in wireless body area networks from a healthcare point of view," in *Proc. 22nd Asia–Pacific Conf. Commun. (APCC)*, Aug. 2016, pp. 523–528.

[5] M. Alam and E. Hamida, "Surveying wearable human assistive technology for life and safety critical applications: Standards, challenges and opportunities," *Sensors*, vol. 14, no. 5, pp. 9153–9209, May 2014.

[6] Y. Rahayu, T. A. Rahman, R. Ngah, and P. S. Hall, "Ultra wideband technology and its applications," in *Proc. 5th IFIP Int. Conf. Wireless Opt. Commun. Netw. (WOCN)*, May 2008, pp. 1–5.

[7] B. Yang, Y. Xu, J. Tong, Y. Zhang, Y. Feng, and Y. Hu, "Tri-port antenna with shared radiator and self-decoupling characteristic for 5G smartphone application," *IEEE Trans. Antennas Propag.*, vol. 70, no. 6, pp. 4836–4841, Jun. 2022.

[8] N. Hussain and N. Kim, "Integrated microwave and mm-wave MIMO antenna module with 360° pattern diversity for 5G Internet of Things," *IEEE Internet Things J.*, vol. 9, no. 24, pp. 24777–24789, Dec. 2022.

[9] Y. Wang, B. Huang, and S. Yan, "A conformal four-antenna module for capsule endoscope MIMO operation," *IEEE Trans. Antennas Propag.*, vol. 70, no. 11, pp. 10270–10285, Nov. 2022.

[10] B. Kumkhet, P. Rakluea, N. Wongsin, P. Sangmahamad, W. Thaiwirot, N. Chudpooti, and C. Mahatthanajatuphat, "SAR reduction using dual band EBG method based on MIMO wearable antenna for WBAN applications," *AEU - Int. J. Electron. Commun.*, vol. 160, pp. 1–16, Feb. 2023.

[11] S. Hongdumnuen, W. Chanwattanapong, and B. Kumkhet, "Multiband thin film antenna for WLAN and LTE MIMO systems," in *Proc. Res., Invention, Innov. Congr., Innov. Electricals Electron. (RI2C)*, Sep. 2021, pp. 139–142.

[12] G.-S. Lin, C.-H. Sung, J.-L. Chen, L.-S. Chen, and M.-P. Houng, "Isolation improvement in UWB MIMO antenna system using carbon black film," *IEEE Antennas Wireless Propag. Lett.*, vol. 16, pp. 222–225, 2017.

[13] D. Sipal, M. P. Abegaonkar, and S. K. Koul, "Easily extendable compact planar UWB MIMO antenna array," *IEEE Antennas Wireless Propag. Lett.*, vol. 16, pp. 2328–2331, 2017.

[14] H. Sakli, C. Abdelhamid, C. Essid, and N. Sakli, "Metamaterial-based antenna performance enhancement for MIMO system applications," *IEEE Access*, vol. 9, pp. 38546–38556, 2021.

[15] J. Deng, S. Hou, L. Zhao, and L. Guo, "A reconfigurable filtering antenna with integrated bandpass filters for UWB/WLAN applications," *IEEE Trans. Antennas Propag.*, vol. 66, no. 1, pp. 401–404, Jan. 2018.

[16] A. Sowmiyadevi and S. Raman, "3-port MIMO antenna for UWB applications with polarization dependency analysis," in *Proc. IEEE Indian Conf. Antennas Propogation (InCAP)*, Dec. 2018, pp. 1–4.

[17] P. Aroonmitr, C. Rakluea, W. Loedhammacakra, P. Rakluea, M. Tangjitjetsada, C. Mahatthanajatuphat, P. Akkaraekthalin, and T. Thianthong, "A minimized thickness of MIMO antenna based on thin film substrates for UWB application," in *Proc. Int. Electr. Eng. Congr. (iEECON)*, Mar. 2023, pp. 268–272.

[18] M. O. Khalifa, A. M. Yacoub, and D. N. Aloi, "A multiwideband compact antenna design for vehicular sub-6 GHz 5G wireless systems," *IEEE Trans. Antennas Propag.*, vol. 69, no. 12, pp. 8136–8142, Dec. 2021.

[19] D. Potti, Y. Tusharika, M. G. N. Alsath, S. Kirubaveni, M. Kanagasabai, R. Sankararajan, S. Narendhiran, and P. B. Bhargav, "A novel optically transparent UWB antenna for automotive MIMO communications," *IEEE Trans. Antennas Propag.*, vol. 69, no. 7, pp. 3821–3828, Jul. 2021.

[20] Z. Zang, A. U. Zaman, and J. Yang, "Single layer dual circularly polarized antenna array based on ridge gap waveguide for 77 GHz automotive radar," *IEEE Trans. Antennas Propag.*, vol. 70, no. 7, pp. 5977–5982, Jul. 2022.

[21] A. Chletsou, J. F. Locke, and J. Papapolymerou, "Vehicle platform effects on performance of flexible, lightweight, and dual-band antenna for vehicular communications," *IEEE J. Microw.*, vol. 2, no. 1, pp. 123–133, Jan. 2022.

[22] A. M. Yacoub, M. O. Khalifa, and D. N. Aloi, "Wide band raised printed monopole for automotive 5G wireless communications," *IEEE Open J. Antennas Propag.*, vol. 3, pp. 502–510, 2022.

[23] L. Kannappan, S. K. Palaniswamy, L. Wang, M. Kanagasabai, S. Kumar, M. G. N. Alsath, and T. R. Rao, "Quad-port multiservice diversity antenna for automotive applications," *Sensors*, vol. 21, no. 24, p. 8238, Dec. 2021.

[24] L. Kannappan, S. K. Palaniswamy, M. Kanagasabai, P. Kumar, M. G. N. Alsath, S. Kumar, T. R. Rao, M. Marey, A. Aggarwal, and J. K. Pakkathillam, "3-D twelve-port multi-service diversity antenna for automotive communications," *Sci. Rep.*, vol. 12, no. 1, pp. 1–22, Jan. 2022.

[25] M. S. Sharawi, "Current misuses and future prospects for printed multiple-input, multiple-output antenna systems [wireless corner]," *IEEE Antennas Propag. Mag.*, vol. 59, no. 2, pp. 162–170, Apr. 2017, doi: 10.1109/MAP.2017.2658346.

[26] M. Manteghi and Y. Rahmat-Samii, "Multiport characteristics of a wide-band cavity backed annular patch antenna for multipolarization operations," *IEEE Trans. Antennas Propag.*, vol. 53, no. 1, pp. 466–474, Jan. 2005.

[27] M. S. Sharawi, "Printed multi-band MIMO antenna systems and their performance metrics [wireless corner]," *IEEE Antennas Propag. Mag.*, vol. 55, no. 5, pp. 218–232, Oct. 2013.

[28] T. Taga, "Analysis for mean effective gain of mobile antennas in land mobile radio environments," *IEEE Trans. Veh. Technol.*, vol. 39, no. 2, pp. 117–131, May 1990.

[29] S. C. K. Ko and R. D. Murch, "Compact integrated diversity antenna for wireless communications," *IEEE Trans. Antennas Propag.*, vol. 49, no. 6, pp. 954–960, Jun. 2001.

[30] A. Desai, C. D. Bui, J. Patel, T. Upadhyaya, G. Byun, and T. K. Nguyen, "Compact wideband four element optically transparent MIMO antenna for mm-wave 5G applications," *IEEE Access*, vol. 8, pp. 194206–194217, 2020.

[31] G. Montisci, G. Mura, G. Muntoni, G. A. Casula, F. P. Chietera, and M. Aburish-Hmidat, "A curved microstrip patch antenna designed from transparent conductive films," *IEEE Access*, vol. 11, pp. 839–848, 2023.

[32] Y.-S. Huang, L. Zhou, Q.-H. Xu, and J.-F. Mao, "A W-band self-packaged SIW-based slot antenna with gain and bandwidth enhancement," *IEEE Trans. Antennas Propag.*, vol. 71, no. 3, pp. 2158–2166, Mar. 2023.

[33] Abdulrahman. S. M. Alqadami, A. E. Stancombe, K. S. Bialkowski, and A. Abbosh, "Flexible meander-line antenna array for wearable electromagnetic head imaging," *IEEE Trans. Antennas Propag.*, vol. 69, no. 7, pp. 4206–4211, Jul. 2021.

[34] H. A. Elmobarak, M. Himdi, X. Castel, S. K. A. Rahim, and T. K. Geok, "Flexible patch antenna array operating at microwaves based on thin composite material," *IEEE Access*, vol. 10, pp. 115663–115672, 2022.

[35] B. Aspe, X. Castel, V. Demange, S. Députier, V. Bouquet, R. Benzerga, R. Sauleau, and M. Guilloux-Viry, "Frequency-tunable slot-loop antenna based on KNN ferroelectric interdigitated varactors," *IEEE Antennas Wireless Propag. Lett.*, vol. 20, no. 8, pp. 1414–1418, Aug. 2021.

[36] J. Li, W. Yang, S. Ma, Q. Xue, and W. Che, "Reconfigurable millimeter-wave tri-band antenna based on VO$_2$-Films-Embedded co-aperture metasurface structures," *IEEE Trans. Antennas Propag.*, vol. 71, no. 4, pp. 3134–3145, Apr. 2023.

[37] A. Patel, A. Desai, I. Elfergani, A. Vala, H. Mewada, K. Mahant, S. Patel, C. Zebiri, J. Rodriguez, and E. Ali, "UWB CPW fed 4-port connected ground MIMO antenna for sub-millimeter-wave 5G applications," *Alexandria Eng. J.*, vol. 61, no. 9, pp. 6645–6658, Sep. 2022.

[38] X.-T. Yuan, W. He, K.-D. Hong, C.-Z. Han, Z. Chen, and T. Yuan, "Ultra-wideband MIMO antenna system with high element-isolation for 5G smartphone application," *IEEE Access*, vol. 8, pp. 56281–56289, 2020.

[39] Z. Chen, X.-T. Yuan, J. Ren, and T. Yuan, "An ultra-wideband MIMO antenna for 5G smartphone," *AEU-Int. J. Electron. Commun.*, vol. 154, pp. 1–7, Sep. 2022.

[40] H. Al-Saif, M. Usman, M. T. Chughtai, and J. Nasir, "Compact ultra-wide band MIMO antenna system for lower 5G bands," *Wireless Commun. Mobile Comput.*, vol. 2018, pp. 1–7, Jun. 2018.

[41] A. B. Dey, S. S. Pattanayak, D. Mitra, and W. Arif, "Investigation and design of enhanced decoupled UWB MIMO antenna for wearable applications," *Microw. Opt. Technol. Lett.*, vol. 63, no. 3, pp. 845–861, Nov. 2020.

PAITOON RAKLUEA received the B.Ind.Tech. degree in electronics technology, the M.Eng. degree in information engineering, and the D.Eng. degree in electrical engineering from the King Mongkut's Institute of Technology Ladkrabang (KMITL), Thailand, in 2000, 2003, and 2009, respectively. Since 2003, he has been with the Rajamangala University of Technology Thanyaburi (RMUTT), Thailand, where he is currently an Assistant Professor. He is also a Lecturer and the Head of the Department of Electronics and Telecommunication Engineering, RMUTT. His current research interests include signal processing, RF/microwave circuits, wideband and multiband antennas, wearable antenna, and thin-film antenna.

NORAKAMON WONGSIN (Member, IEEE) received the B.Eng., M.Eng., and Ph.D. degrees in electrical engineering from the King Mongkut's University of Technology North Bangkok (KMUTNB), Thailand, in 2009, 2012, and 2019, respectively. Since 2012, he has been a Lecturer with the Department of Electronics and Telecommunication Engineering, Faculty of Engineering, Rajamangala University of Technology Thanyaburi (RMUTT), Thailand. His research interest includes wideband and multiband small antennas for communication applications.

CHATREE MAHATTHANAJATUPHAT (Member, IEEE) received the M.Eng. degree from the Rosenheim Technical University of Applied Sciences, Germany, in 2003, and the Ph.D. degree from the King Mongkut's University of Technology North Bangkok (KMUTNB), Thailand, in 2009. In 2017, he was appointed as a Lecturer (Associate Professor) with the Department of Electrical Engineering, KMUTNB. His main research interests include the designing of small antennas using the fractal geometry concept and digital signal processing for communication applications.

CHAWALIT RAKLUEA (Member, IEEE) received the B.Eng. (Hons.) and M.Eng. degrees in electrical engineering (telecommunication) from the King Mongkut's University of Technology North Bangkok (KMUTNB), Thailand, in 2009 and 2012, respectively, where he is currently pursuing the Ph.D. degree in electrical engineering. Since 2012, he has been a Lecturer with the Rajamangala University of Technology Thanyaburi (RMUTT), Thailand. His research interests include wireless power transmission, metamaterials, metasurface, and antenna technology.

PONGSATHORN AROONMITR was born in Chanthaburi, Thailand, in 1995. He received the B.Eng. and M.Eng. degrees from the Rajamangala University of Technology Thanyaburi (RMUTT), Thailand, in 2018 and 2023, respectively. He has been with The National Broadcasting and Telecommunications Commission of Thailand (NBTC). His research interests include thin film antennas, UWB antennas, MIMO antennas, and wireless communications.

WANCHALERM CHANWATTANAPONG received the B.Eng. degree in electrical engineering from Khon Kaen University, Thailand, in 2001, and the M.Eng. degree in information engineering from the King Mongkut's Institute of Technology Ladkrabang (KMITL), Thailand, in 2007. Since 2010, he has been a Lecturer with the Rajamangala University of Technology Thanyaburi (RMUTT), Thailand. His current research interests include the IoT, machine learning, and thin-film antenna.

NONCHANUTT CHUDPOOTI (Member, IEEE) received the B.Sc. degree (Hons.) in industrial physics and medical instrumentation and the Ph.D. degree in electrical engineering from the King Mongkut's University of Technology North Bangkok (KMUTNB), in 2012 and 2018, respectively. He was appointed as a Lecturer with the Department of Industrial Physics and Medical Instrumentation, Faculty of Applied Science, KMUTNB, in 2018. His main research interests include the application of microwave microfluidic sensors, millimeter-wave substrate-integrated circuit applications, and substrate-integrated waveguide applications. He was a recipient of the Best Presentation Award from Thailand–Japan Microwave, in 2015 and 2018, and the Young Researcher Encouragement Award, in 2016.

THINNAWAT JANGJING received the B.Eng. degree in electronics and telecommunication engineering and the M.Eng. degree in electrical engineering (telecommunication) from the Rajamangala University of Technology Thanyaburi (RMUTT), Thailand, in 2009 and 2012, respectively. He has been a Lecturer with the Faculty of Engineering, RMUTT. His research interests include renewable energy, wearable antenna IoT, and LoRA applications.

• • •